International Journal of Heat and Mass Transfer 113 (2017) 153–165

Contents lists available at ScienceDirect

International Journal of Heat and Mass Transfer

journal homepage: www.elsevier.com/locate/ijhmt

Moving heat source in a confined channel: Heat transfer and boiling in endovenous laser ablation of varicose veins

Amit de Boer [a], Jorge L.G. Oliveira [b], Cees W.M. van der Geld [c,*], Wendy S.J. Malskat [d], Renate van den Bos [d], Tamar Nijsten [d], Martin J.C. van Gemert [e]

[a] Department of Mechanical Engineering, Eindhoven University of Technology, Eindhoven, The Netherlands
[b] Technology Center, Federal University of Santa Catarina, Joinville, SC 89218-000, Brazil
[c] Department of Chemical Engineering and Chemistry, Eindhoven University of Technology, Eindhoven, The Netherlands
[d] Department of Dermatology, Erasmus University Medical Center, Rotterdam, The Netherlands
[e] Department of Biomedical Engineering and Physics, Academic Medical Center, University of Amsterdam, Amsterdam, The Netherlands

ARTICLE INFO

Article history:
Received 30 November 2016
Received in revised form 10 April 2017
Accepted 17 May 2017

Keywords:
Boiling
Blood
Water
Moving heat source
Laser ablation
Endovenous laser ablation of varicosities

ABSTRACT

Motion of a moving laser light heat source in a confined volume has important applications such as in endovenous laser ablation (EVLA) of varicose veins. This light heats up the fluid and the wall volume by absorption and heat conduction. The present study compares the flow and temperature fields in a horizontal tube of 4 mm inner diameter in three idealizations of the EVLA procedure: water with a bare fiber tip, water with a carbonized layer on the fiber tip, and blood. Without boiling, the convection patterns in water and blood are similar and Grashof numbers are high enough to guarantee buoyancy induced flow and axial mixing, while preserving some stratification. A carbonized layer at the fiber tip promotes boiling in water at moderate laser powers. Boiling bubbles in water rapidly detach from the tip, with or without a carbonized layer, and promote mixing and a locally homogeneous temperature field. At 15 W laser power and 4 mm/s pullback speed in blood, a gas bubble may be formed that sticks at the fiber tip, causing strong local heating and possibly fiber damage.

1. Introduction

The fluid motion created by the passage of a propagating heat source has many interesting applications. The case of a propagating *periodic* heat source has become known as the 'moving-flame' phenomenon, after Fultz et al. [1] who performed the first experiments of this kind with a Bunsen flame. Other types of fluid motion created by moving heat sources are more commonly found in geophysics. Examples are the earth's super rotation, see Rishbeth [2], and the origin of tornados, Stern [3]. The latter examples motivated Douglas et al. [4] to carry out a study with a heat source rotating around an annular volume filled with water. Another interesting example is found in welding research. In this case, fluid flow is accompanied by a phase change and research aims to minimize the size of the heat-affected zone and to reduce unwanted effects such as distortion and residual stress; see Yang et al. [5], Ye and Chen [6], and Karimipour et al. [7]. The final quality of the weld is dependent on the hydrodynamics in the liquid region and the energy transfer in the surrounding zone; see Mundra et al. [8].

The above studies were performed in relatively large volumes of flow. Since a decade or two, moving heat sources are applied in the medical field in far more limited volumes of liquid during the laser treatment of varicose veins. Endovenous Laser Ablation (EVLA) treatment consists of introducing a catheter into a vein that has a typical diameter of 5–12 mm. The catheter is used to transport a fiber consisting of a silica core and polymer cladding. The fiber guides laser light that emanates from the tip of the fiber and heats up the blood in the vein. A tumescent fluid is usually inserted to anesthetize the nerves surrounding the vein and to compress the vein. The laser light heats up the vein by a variety of heat transfer mechanisms: absorption in blood and vein tissue, conduction, convection and boiling; see Malskat et al. [9]. Heat is transferred towards the vein wall and causes the vein to be irreversibly injured. According to Pearce and Thomsen [10] irreversible injury of the varicose vein is achieved if a threshold temperature of approximately 75 °C occurs during 1 s, or 70 °C during 10 s.

Although the treatment of varicosities by EVLA has a high success rate with minimal complications, the main mechanisms of action is still under discussion. Mordon et al. [11] initially proposed

* Corresponding author.
E-mail addresses: jorge.goes@ufsc.br (J.L.G. Oliveira), C.W.M.v.d.Geld@tue.nl (C.W.M. van der Geld), m.j.vangemert@amc.uva.nl (M.J.C. van Gemert).

http://dx.doi.org/10.1016/j.ijheatmasstransfer.2017.05.068
0017-9310/

Nomenclature

D	pipe diameter
EVLA	endovenous laser ablation
g	gravity acceleration
Gr	Grashof number
L_c	characteristic length scale
r	radial coordinate
R	pipe radius
Re	Reynolds number
t	time
T	temperature
u	pullback speed
x	streamwise coordinate
y	vertical coordinate

Greek symbols

β	coefficient of thermal expansion
ν	kinematic viscosity

Subscripts

max	maximum

an optical-thermal response to scattered laser light. Also heat diffusion from the hot fiber tip was considered to be significant; see van den Bos et al. [12]. Fiber tips can reach temperatures of over 800 °C (see Verdaasdonk et al. [13] and Weiss [14], for example), as a result of the absorbing thin layer of carbonized blood which is deposited on the fiber tip during EVLA treatment, Amzayyb et al. [15]. Direct contact between the tissue and the fiber tip was found to contribute to vein wall perforations; see Vuylsteke et al. [16]. The presence of condensing boiling bubbles was commented by Fan and Anderson [17], Disselhoff et al. [18] and Proebstle et al. [19], but not considered an essential EVLA mechanism. However, van der Geld et al. [20] have accredited boiling as an important heat transfer mechanism resembling the action of a heat pipe. They demonstrated the occurrence of boiling bubbles emerging from pores within the hot fiber tip and traveling over a length of about 20 mm before condensing. The present study is an experimental simulation of EVLA and it will be shown that boiling is indeed an essential EVLA mechanism. The conditions for the occurrence of boiling will be explored in this work.

It is obvious that boiling occurs if a heat source moving slowly through a fluid is powerful enough. Confined boiling exhibits special properties as compared to boiling in wide channels. Flow boiling in mini-channels, for example, is renowned for the occurrence of backflow and blocking of the channel by a vapor pocket with a length of 1 to several diameters; see Rops et al. [21,22]. Confined pool boiling has shown the occurrence of near stagnant bubbles and bubbles adhering to a horizontal surface; see Passos et al. [23,24]. The present study will show under what circumstances boiling will occur in a mini-channel (4 mm inner diameter) and that the type of convection flow introduced by the moving heat source depends strongly on whether boiling occurs or not. Both blood and water will be examined.

When a fiber tip emits intense light when moving through blood, the tip becomes carbonized, Amzayyb et al. [15] and Van den Bos et al. [12]. The level of carbonization changes during the process and the final level of carbonization is *a priori* unknown. In order to mimic the physics of this process with water, two levels of idealization are possible:

- A laser light emitting bare fiber tip moving at constant speed in water;
- A laser light emitting fiber tip with a carbonized layer attached to it moving at constant speed in water.

In the present paper, both idealizations will be studied in an experimental model of a vein. In addition, also

- A laser light emitting initially bare fiber tip moving at constant speed in blood will be examined.

The main advantage of water as a test fluid is its optical transparency and the possibility of visualizing boiling bubbles. An additional advantage of water as a mock-up fluid for blood is the fact that most physical properties of water come close to those of blood. The main difference is the light absorption coefficient, which is lower by a factor of 11 at 980 nm, the laser wavelength used in our experiments.

Since quite high heating powers of up to 25 W will be considered, temperature gradients are to be expected that may cause natural convection in a confined cylindrical volume with a length of 84 mm and an inner radius of 2 mm where a laser fiber is pulled at constant speed u. We will show below in the RESULTS section that temperature differences nearby the laser fiber tip are typically 20 °C. The flow situations encountered in this study may therefore be categorized with the aid of a Grashof number, Gr. In order to define a typical Grashof number, let the characteristic length scale in the direction opposite to the direction of gravity, the y-direction, be denoted with L_c. This length must correspond to the vertical distance over which the main temperature drop takes place. Distance L_c will in Section 2 and subsequent sections of this paper be taken equal to the radius of the tube, which is 2 mm. A more conservative estimate would be half the radius (1 mm), based on the argumentation that the resulting buoyancy flow must bend direction from vertical to horizontal at a distance from the tube wall. This conservative estimate will be used in Section 1, below, in order to make sure the importance of buoyancy flows in the experiments of this paper. Let furthermore u be the pullback speed of the heat source along the central axis of a horizontal tube with radius R, ν the kinematic viscosity, $\boldsymbol{g}$ the gravity acceleration, β the coefficient of thermal expansion, T temperature. The typical velocity induced by buoyancy in the y-direction over height L_c is given by $v_{tb} = \sqrt{\boldsymbol{g}\beta(T(y_t) - -T(y_c))L_c}$, if dissipation is discarded. Temperatures at y-positions y_c and y_t refer to the centerline of the horizontal tube and to a vertical position displaced by the height L_c, in that order. If this velocity is related to the pullback speed, u, the following modified Grashof number, Gr, is obtained:

$$Gr = \boldsymbol{g}\beta(T(y_t) - T(y_c))L_c/u^2 \tag{1}$$

If the typical velocity of diffusion of liquid momentum, ν / L_c, is used to replace u a familiar form of the Grashof number is retained:

$$g\ \beta(T(y_t) - T(y_c))L_c^3/\nu^2 \tag{2}$$

It is well known that when the ratio of Grashof to Reynolds numbers squared, equal to Eq. (1) with u seen as the convection velocity that occurs in the Reynolds number, exceeds 10, forced convection effects are negligible; see Çengel [25]. Because of this, whenever Gr exceeds 10, convection effects of the pullback speed are negligible.

If convective cooling by the liquid that is moved by the fiber tip heat source dominates heat transfer, the temperature difference ($T(y_t) - T(y_c)$) depends on u. With a constant heat flux and the Colburn relation for convective cooling, Çengel [25], it is easily shown that ($T(y_t) - T(y_c)$) is then proportional to $u^{-0.8}$. However, it is *a priori* unclear whether convection is dominant and constant heat flux premises can be made. If light absorption is dominant, temperature differences may be independent of velocity. That is why in the present study ($T(y_t) - T(y_c)$) will be based on experiments.

For water, β is about 3.10^{-4} K^{-1}. Estimates for Eq. (2) with water and L_c = 1 mm and with a typical temperature difference of our measurements (around 20 K) are in the range of 5–50. This means that in the absence of an effect of flow convection due to the pulling back of the fiber, natural convection is expected to affect the temperature field in the channel. In the present study, definition (1) will be used to assess the importance of natural convection with respect to forced convection. With detaching boiling bubbles, an even better mixing and a better heat transport is anticipated. Whether this is actually the case will also be investigated.

The focal points of this study are the answers to the following questions: How are flow and temperature fields induced in a tube by a moving heat source if no boiling occurs? Does stratification occur if the tube is horizontal? What are the differences between water and blood? Are transient phenomena significant? How does boiling affect the answers to the previous questions? How is bubble detachment taking place in water and blood? Which conditions are favorable for EVLA?

The organization of the manuscript is as follows. First, the experimental set-up and notations used are introduced in the METHODS Section 2. Next, in the RESULTS Section 3, visualizations and temperature measurements in both water and blood without boiling are presented in Section 3.1. In Section 3.2, temperature and flow fields with boiling but without the occurrence of gas bubbles are examined. In Section 3.3, measurements in blood with gas bubbles are presented and analyzed. Finally, a DISCUSSION is presented in Section 4.

2. Methods

2.1. Experimental set-up

A schematic overview of the set-up is presented in Fig. 1. A reservoir (Fig. 1a) contains a test section (Fig. 1b and c) made of quartz. The temperature of the reservoir that holds the test section is controlled by a Lauda thermal bath. The test section has an external diameter of 6 mm and an inner diameter of $D = 2R = 4$ mm. Its length is 84 mm. The quartz holder of the fiber that is made to move through the center of the test section has an inner diameter of 0.7 mm and is welded to the test section, on the right hand side of it. The commercially available fiber has a silica core with inner diameter of 0.4 mm and a polymer cladding with external diameter of 1.0 mm. The cladding was removed from the fiber in order to make it possible to move the fiber through the capillary. The strength of the resulting bare fiber was found to be sufficient to keep it centered along the length of the test tube over 84 mm (Fig. 1a). The fiber tip deflection from the horizontal was less than 0.2 mm.

Six thermocouples can be positioned normal to the wall at various heights within the measurement volume. Numbers (1, 2 and 3) and symbols (□, ○, ▽ and △) in Fig. 1b and c indicate the positions of the tips of the thermocouples. The thermocouples are of type K with a measurement uncertainty of 0.5 °C, which have been calibrated with a thermal bath. Dedicated holders for thermocouples were made out of stainless steel with a tip made of Delrin polymer material. This contraption warrants no damage of the quartz pipe, good stiffness and flexible positioning of the thermocouples.

Recordings are made with a Photron "High-SpeedStar" camera with 12-bit grayscale CMOS sensor and a resolution of 1024 × 1024 pixels, focused on the fiber tip inside the tube. A linear electric motor is used to pull the fiber at constant speed through the measurement section. A triggering system synchronizes the motor, laser power and temperature and camera recordings.

2.2. Experimental procedure

A Cartesian coordinate system with the origin at the open end of the quartz pipe is adopted (Fig. 1); x is in horizontal direction and y in vertical direction (Fig. 1b and c). The pullback direction of the fiber is along the line $y = 0$. Schematics like the one of Fig. 1 will be used with all figures and tables below to elucidate the positions of thermocouples and laser fiber. The thermocouples are positioned at three axial x-positions; see Fig. 1: 40, 60 and 70 mm. The starting position of the fiber is at $x = 24$ mm. At each of these x-positions, temperatures were measured at four heights: y = −1.5, −1, 1 and 1.5 mm (Fig. 1b and c). Recordings at y = +1 mm are indicated by the square □, those at −1 mm by the circle ○. Temperatures measured at y = +1.5 mm are denoted by ▽ and those at −1.5 mm by △. In each test, temperature recordings were performed in only two y-positions: −1 and +1 mm; or −1.5 and +1.5 mm. The closed end of the quartz pipe is at 84 mm, the distance between the third axial thermocouple at 70 mm and the closed end is only 3.5 times the tube diameter $D = 4$ mm, see Fig. 1b and c.

Each temperature measurement presented below is an average of 5 consecutive measurements where synchronization of the 5 curves was done by placing the maximum of the 1st T-curve, at upper thermocouple 1, at 6 s. The initial temperature in the container and the measurement section was homogeneous and adjusted to 38 °C.

Experiments were performed under 15 conditions based on the variation of four variables: (a) fluid composition (water or blood), (b) presence or absence of a carbonized layer on the fiber tip, (c) laser power (5, 10, 15 or 25 W), and (d) pullback speed (2 or 4 mm/s). Three of these 15 conditions were only applicable for blood: 4 mm/s; initially bare tip; 5, 10 or 15 W. At a pullback speed of 2 mm/s, measurements in blood were impossible for any laser power because the thermocouples broke down. At any pullback speed, measurements in blood were impossible at 25 W laser power, for the same reason. The settings for laser power and pullback speed were chosen based on clinical values; see Van den Bos et al. [12].

Experiments with the presence of a carbonized layer on the fiber tip were made possible as follows. The laser fiber was inserted in fresh blood at room temperature. A laser power of 20 W was applied for 20 s. Subsequently, the laser fiber was removed and cooled down to room temperature for 20 s. The coagulum formed, *i.e.* a blood clot, was wiped off with a piece of paper, leaving the carbonized layer on the tip of the probe. This procedure was repeated twice.

Experiments with blood instead of water required filling the vessel with blood obtained from a slaughter house and kept in refrigeration for only a limited period of time, one week maximum. Coagulum formation, particularly at the thermocouple tip, during the experiment was avoided by replacing the blood in each experiment. Blood was put in a closed beaker floating in a thermal bath until reaching human body temperature of 38 °C uniformly. Only then it was inserted in the test section by a syringe. During the experiments, the recirculating water for thermal control was replaced regularly to prevent contamination.

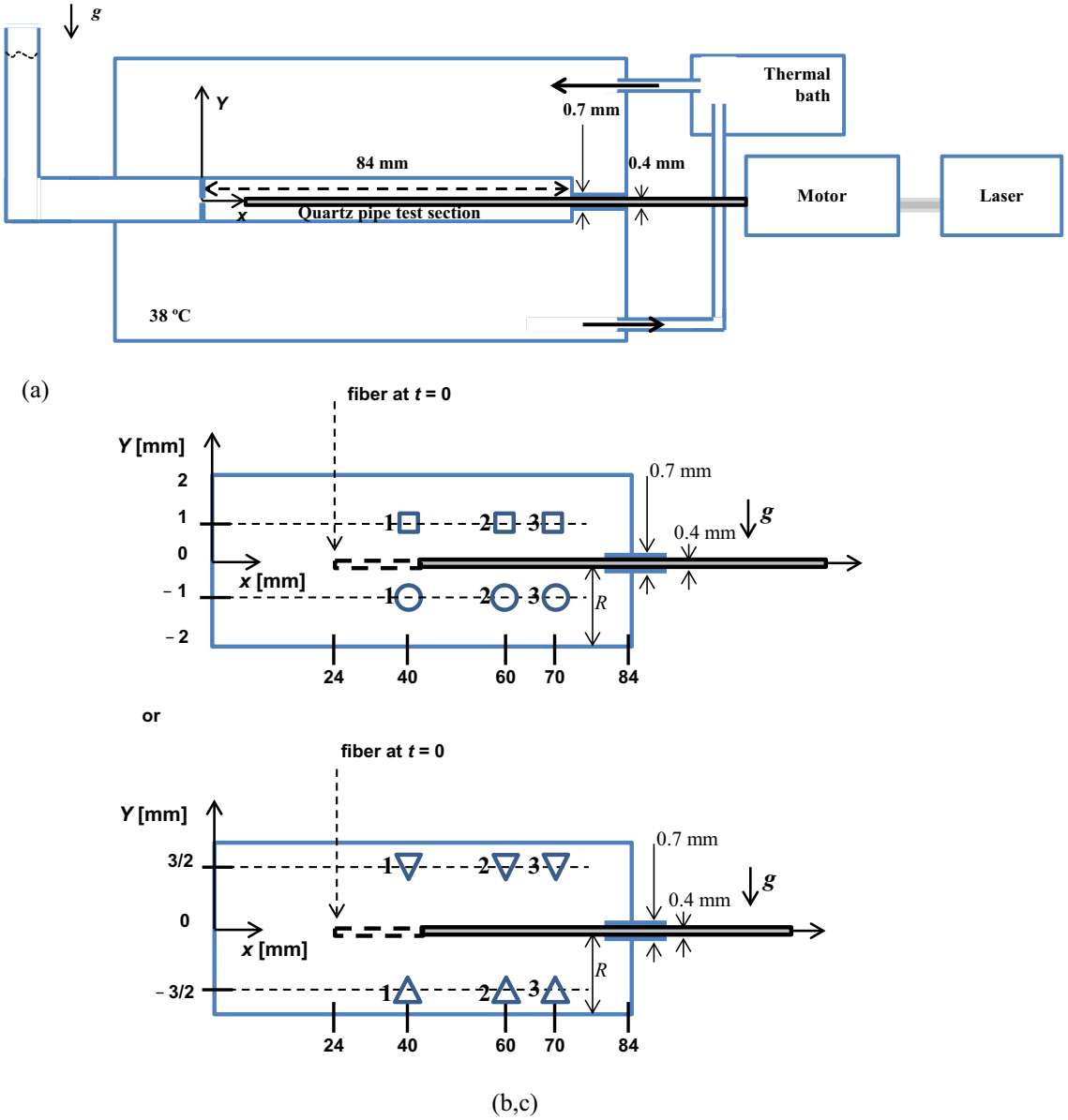

Fig. 1. Schematic overview of the measurement setup. (a) Overall set-up; (b, c) test section. Numbers 1, 2 and 3 indicate the *x*-position of the thermocouples. In (b) squares and circles indicate that the *y*-position is at +1.0 mm (□) or at −1.0 (○). In (c) triangles indicate that the *y*-position is at +1.5 mm (▽) or at −1.5 (△).

Absorption properties of laser light in blood and water are important for the interpretation of the measurements. In blood, chromophores occur. The most important ones are hemoglobin (Hb) and oxyhemoglobin (HbO_2). In our experiments, blood was in contact with air which implies that it became oxygenated, hence, our blood primarily contained oxyhemoglobin as chromophore. The HbO_2 absorption spectrum together with that of H_2O is plotted in Fig. 2; the wavelength used in this study is 980 nm. Although it would have been preferred to test blood and water at wavelengths where the absorption coefficients of HbO_2 and H_2O are more alike, the wavelength of 980 nm used in EVLA was applied. We emphasize that the selection of wavelength for EVLA treatment has been subject of much debate; see Poluektova et al. [28]. It will be shown that the most striking difference occurring in the experiments with these fluids is related nevertheless to boiling dynamics at the fiber tip as a result of the blood chemical composition. The difference in boiling dynamics will occur even if the absorption coefficients of the fluids would be matched.

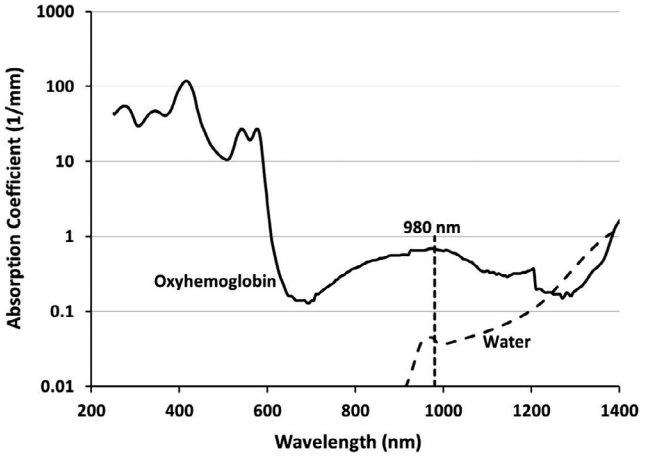

Fig. 2. The absorption coefficients of water and oxyhemoglobin (HbO_2). Data for HbO_2 are from Bosschaard et al. [26]; those for water from Hale and Querry [27].

The volume heated by laser light is confined by the total angle of radiation of the fiber, which amounts to about 30° with the horizontal in water and blood. The penetration depth of the light also confines this volume. Because of the large difference in absorption the volume heated by radiation is much smaller for blood than it is for water. As a consequence, higher temperatures are expected with blood close to the fiber tip.

2.3. Notation used throughout this paper

The main measurement results are temperature histories at various locations and visual observations of hot fluid parts, with the aid of a dye, bubbles and at the various fiber positions.

Fig. 3 shows two temperature histories with the definitions of the maximum temperature $T_{max,1}$ at two y-locations, $T_{max,1,\square}$ and $T_{max,1,\bigcirc}$. The corresponding times are $t(T_{max,1,\square})$ and $t(T_{max,1,\bigcirc})$. The difference in temperature of the two thermocouples at the first time, $t(T_{max,1,\square})$, is denoted by ΔT_{max}. Definitions for T_{max} at the two other thermocouples, T_{max2} and T_{max3}, at $x = 60$ mm and at $x = 70$ mm, are similar. The first time that the temperature of a therocouple at x-position 1 starts increasing is denoted as $t_{rise,1}$. The one for the lower thermocouple, ○, is shown in Fig. 3a. The definitions of times $t_{rise,2}$ and $t_{rise,3}$ are similar.

The main features of all measured temperature-time histories are collected in the tables of Appendix A. Each table is for a certain y-value of thermocouples, which eliminates the need to use the graphic symbols □, ○, ▽ and △ mentioned above; annotation like $t(T_{max,1})$ suffices in these tables. The times given in Appendix A enable to define velocities in the following way. The times $t(T_{max,1})$ and $t(T_{max,3})$ presumably correspond to the times the hot fiber tip passes the locations 1 and 3. If there is an offset, it is assumed to be the same at both locations; the validity of these assumptions will be examined below. Since the axial distance between couples

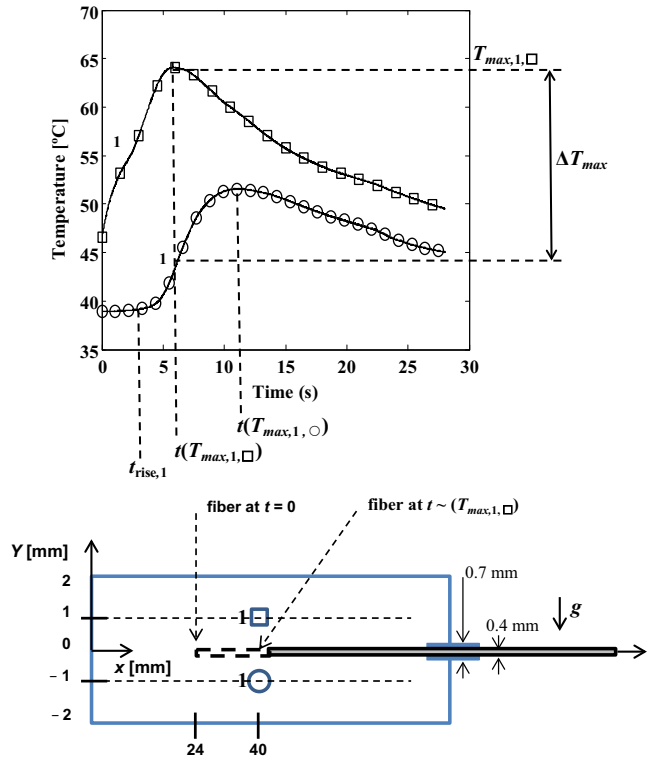

Fig. 3. Schematics of temperature-time histories based on actual measurements. The annotation 1 refers to the two thermocouples at position 1, which is at $x = 40$ mm. Note that the lower figure is not to scale.

1 and 3 is 0.03 m, the corresponding transit velocity, v_{13}, is in m/s given by

$$v_{13} = 0.03/(t(T_{max,1}) - t(T_{max,3})). \quad (3)$$

Similarly, a vertical velocity can be estimated from the readings of two thermocouples at the same axial x-position. However, in this case the distance traveled is unknown. A plausible streamline is one that follows the circumference of the tubular channel, rather than a straight line. For this reason the distance traveled is set to 3 mm for two thermocouples at a vertical distance of 2 mm. This yields the following mean velocity from the thermocouple on **t**op to the one at the bottom:

$$v_{tb} = 0.003/(t(T_{max,1,\bigcirc}) - t(T_{max,1,\square})). \quad (4)$$

Finally, the Grashof number, Gr, defined by Eq. (1), will be used to assess the importance of natural convection relative to convection induced by the pulling back of the fiber. Temperature gradients are estimated as $\Delta T/\Delta y$ with ΔT the instantaneous difference in temperature in vertical direction over distance Δy. The distance Δy is taken here to be equal to $R = 2$ mm if thermocouples □ and ○ are used for ΔT, or to 1.5 $R = 3$ mm if thermocouples ▽ and △ are used to assess ΔT.

3. Results

3.1. Temperature and flow fields without boiling

This condition occurs with water and a fiber tip without carbonization, named "bare tip", at laser powers of 5 W (pullback speed of the laser being 2 or 4 mm/s) or of 15 W (pullback speed 4 mm/s). This condition also occurs with water and a fiber tip with carbonization, named "carbon tip", at laser power 5 W (2 or 4 mm/s).

3.1.1. Features common in all experiments

Fig. 4 shows typical temperature-time histories for water, bare fiber tip, laser power of 5 W and pull back speed of 2 mm/s. The features of this figure that are typical for all temperature measurements will be analyzed in detail first.

At each thermocouple position, the time difference between the time the temperature starts increasing, t_{rise}, and the occurrence of the maximum temperature, $t(T_{max})$, is about constant and equal to the distance between the initial location of the fiber tip divided by the pullback velocity. This is confirmed by values of the velocity v_{13} that are about equal to the pullback velocity in all cases, see Table 1. This Table 1 summarizes characteristics of the measurement data from 11 of the 15 experimental conditions that facilitate interpretation of the results; the main measurement data are in Appendix A. Of course, velocities v_{12} based on the time of travel from thermocouples 1 to 2 are also equal to the pullback speed. The fact that v_{12}, v_{13} and u are equal confirms that the maximum temperature occurs when the fiber tip passes by. Velocity v_{tb} is based on the fictitious fluid travel distance of 3 mm between the two thermocouples at the same position 1. Temperatures are the averages of 5 consecutive measurements. Grashof numbers are presented below, calculated from Eq. (1), with the pullback velocity, u, as indicated in the first column (2 or 4 mm/s) and the length scale of 2 mm (vertical distance in position 1 between symbols □ and ○). The temperature difference in Eq. (1), $T(y_t) - T(y_c)$, is given by the temperature difference at time $t(T_{max,1})$, i.e. ΔT_{max}. Measured data of flow fields with vapor and gas bubbles are also included in Table 1.

A second common feature in most measurements is the ratio of $T_{max,2}$ to $T_{max,1}$.and that of $T_{max,3}$ to $T_{max,2}$. The first ratio is exceeding 1, the second is less than 1, see Fig. 4. The latter is a consequence of the averaging procedure and the steep temperature gradients in

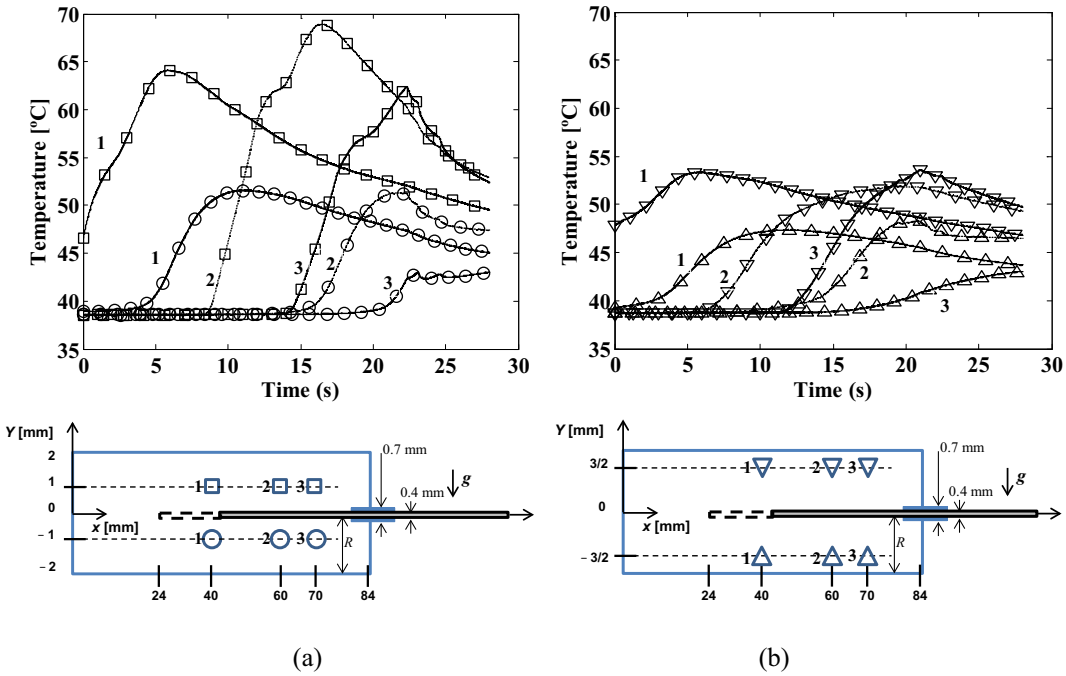

Fig. 4. Temperature-time histories measured in water with a bare fiber tip at relatively low power (5 W) and with pullback speed of 2 mm/s. Figure (a) shows those relatively close to the centerline, at positions y/R = +0.5 and −0.5. Figure (b) those further away from the centerline, at positions y/R = +0.75 and −0.75.

Table 1
Measured and derived data of 11 experimental conditions. Typical velocities and maximum temperatures of thermocouples positioned on top of the fiber tip line (□), and fairly close to it, are given for three positions, labeled 1, 2 and 3 at consecutive downstream positions; see Fig. 4a.

Experiment	v_{13}	v_{tb} [b]	$T_{max,1}$	$T_{max,2}$	$T_{max,3}$	ΔT_{max}	Gr
5 W; 2 mm/s; bare tip; water	1.9	0.6	64	69	62	21	31
15 W; 2 mm/s; bare tip; water	1.9	3.0	92	100	87	40	58
25 W; 2 mm/s; bare tip; water	2.1	1.0	90	100	92	30	44
5 W; 4 mm/s; bare tip; water	3.3	1.0	53	57	52	16	6
15 W; 4 mm/s; bare tip; water	3.3	1.0	72	86	73	30	11
25 W; 4 mm/s; bare tip; water	3.3	1.0	74	101	77	19	7
5 W; 2 mm/s; carbon tip; water	1.8	0.2	68	77	69	38	55
15 W; 2 mm/s; carbon tip; water	1.9	0.6	82	101	83	17	25
25 W; 2 mm/s; carbon tip; water	1.8	0.5	92	102	93	22	32
5 W; 4 mm/s; bare tip; blood	3.8	1.5	62	54	58	20	7
15 W; 4 mm/s; bare tip; blood	3.3	0.6	184	132	108	40[a]	14[a]
	mm/s	mm/s	°C	°C	°C	°C	–

[a] Maximum blood temperature has been taken to be 100 °C. More information in Section 3.3.
[b] Travel distance set to 3 mm.

the individual registrations of temperature-time histories. Synchronizing peak 1 at the same time in five measurements turns out to locate the five peaks at position 3 at different times such that the average temperature-time history shows a broader peak with a lower peak value. The observation that the first ratio of maximum temperatures exceeds 1 can be explained as follows.

Induced convective motion plays an important role, as evidenced by the Grashof number of about 38 for the case of Fig. 3, see Table 1. Thus Gr exceeds 10 by far and buoyancy flows are expected to dominate due to the pulling back of the fiber. Induced convection increases the fluid temperature around position 2 before the fiber tip arrives, at $t(T_{max,2})$. In the case of water with a bare tip, all radiation power results in heat absorbed by the water, which adds to the already existing fluid temperature. Dedicated experiments with ink have been performed to confirm this hypothesis. With ink injected just in front of a stagnant fiber tip, the ink spread upward and to both sides once the laser was switched on. Also with a moving fiber tip, ink was found to move upstream, *i.e.* in the direction in which the fiber is moving. Even when the fiber was stopped at 4 mm downstream from the top thermocouple at position 2, □, *i.e.* at x = 56 mm, a considerable rise in temperature (to 63 °C) was observed. The same is of course seen in Fig. 4a, since the maximum value of the curves 1 occurred when the fiber tip passed by. Hot fluid is driven by buoyancy to the thermocouple and this heating is longer for thermocouple 2 than for thermocouple 1, which explains the difference in maximum temperatures.

A third common feature seen in Fig. 4 is that at each axial position, temperatures rise earlier at the top of the horizontal tube that at the bottom; compare the two curves with number 1 to those with number 2. Hot fluid parts must travel from the top to the bottom of the horizontal tube and the velocity v_{tb} indicates the net effective transport velocity. The origin of all these induced velocities is buoyancy, as explained from the high Grashof numbers

above. All velocities v_{tb} in Table 1 are on the order of 1 mm/s irrespective of the pullback velocity. The horizontal component of the induced flow, $\boldsymbol{v_{13}}$, must exceed 2 mm/s in order to explain the observed traveling upstream, but the downward vertical component, a consequence of mass conservation and the limited volume of the tube, occurs in a larger volume of space and is therefore smaller on the average. This is confirmed by the temperature-time histories at location 3, see Fig. 4. This location is fairly near to the downstream end of the half-closed quartz pipe and the closed end of the pipe blocks the flow and bends the hot fluid flow back in downstream direction, *i.e.* in the negative *x*-direction. As a result, maxima of upper and lower thermocouples at position 3 nearly coincide in time.

The instantaneous and local standard deviation, a measure for the accuracy of the temperature determination, is as low as 2 °C when no boiling occurs and can be as high as 10 °C with boiling occurring near the thermocouples that are located above the centerline and close to the fiber tip. Essentially the same variations for blood and water are found.

This was the final observation that pertains to all temperature histories measured and in the remainder of this paper only the differences between various process conditions will be examined.

3.1.2. Temperature histories in water with bare tip, 5 W (2 or 4 mm/s) or 15 W (4 mm/s)

In this section only measurements without boiling are discussed. With powers up to 15 W, no boiling was observed with a bare tip, while for 15 W it was observed only in the case of 2 mm/s. In the no-boiling case of Fig. 4 at 5 W, the temperature gradients are clearly larger near the top (compare ▽ and □ in Fig. 4a and b) than near the lower part of the tube (compare ○ and △ in Fig. 4a and b). It is concluded that without boiling, stratification occurs and the temperature field in not homogeneous.

A clear effect of increasing the pullback speed is the reduction of local temperatures and of temperature differences in vertical direction, ΔT_y. A 25–40% decrease in ΔT_{max} is found with an increase of *u* from 2 to 4 mm/s, see Table 1. Typical Grashof numbers at 4 mm/s are about one sixth of corresponding ones at 2 mm/s (Table 1), showing that buoyancy induced convective currents are less significant as in the 2 mm/s-case, although they preserve the other characteristics mentioned in the above.

As in the above case for 5 W, a bare fiber tip in water at 15 W laser power and at 4 mm/s pullback speed creates temperature gradients at the upper part of the pipe that exceed those in the lower part of the pipe. Although boiling did not occur in this experiment, some temperatures at $y/R = +0.5$, □, and position 2 came close to 100 °C in this case (results not shown).

3.1.3. Temperature histories in water with a carbon tip, 5 W (2 or 4 mm/s)

With 5 W and with carbonized layer, temperature gradients in the vertical direction are larger than those without the carbonized layer; compare the temperature profiles in Figs. 4a and 5. Heating of the fluid with a carbonized layer yields a higher temperature difference and higher Grashof number at 5 W; see Table 1.

3.2. Temperature and flow fields with boiling but without gas bubbles

This condition occurs with water and a fiber tip *without* carbonization at a laser power of 15 W (pullback speed of the laser being 2 mm/s) or of 25 W (pullback speed 2 or 4 mm/s). This condition also occurs with water and a fiber tip *with* carbonization at laser power 15 or 25 W (2 or 4 mm/s). Furthermore, this condition occurs with blood at 5 and 10 W (4 mm/s).

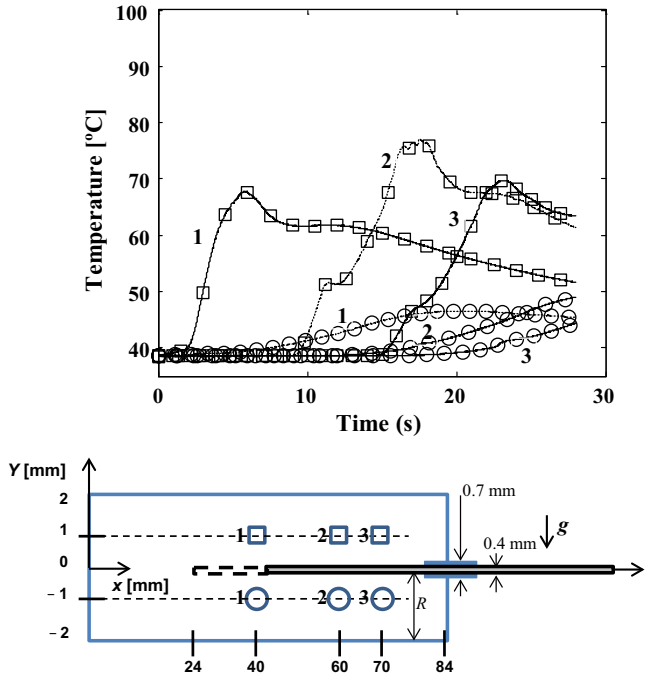

Fig. 5. Temperature-time histories measured in water with a fiber tip with a carbon layer at relatively low power, 5 W; pullback speed is 2 mm/s. Positions are relatively close to the centerline, at positions $y/R = +0.5$ and -0.5.

3.2.1. Typical temperature histories in water with a bare tip, 15 W (2 mm/s) or 25 W (2 or 4 mm/s)

A typical visualization of boiling phenomenon and typical temperature histories with a bare fiber tip in water at 25 W laser power and 2 mm/s pullback speed are presented in Figs. 6 and 7, respectively. Even after averaging of 5 time series, the results of Fig. 7 exhibit quite significant high-frequency fluctuations in the course of time. Visual observations showed the occurrence of bubbles under these circumstances. So it turns out that the occurrence of boiling can be inferred from the fluctuations in time of the temperatures. The boiling bubbles start as big ones near the fiber tip, leave the tip and subsequently condense to smaller sizes further away in the colder flow areas. In Fig. 6b, the tip is close to the end of the tube at ~28 s after switching on the laser. Just after bubble detachment condensation sets in and in a distance of about 15 mm the bubbles can fully disappear.

As compared to the non-boiling case of Section 3.1, temperature differences in vertical direction at a certain *x*-position in the measurement volume are about the same (5 degrees) in both cases at times exceeding 10 s; compare the two curves labeled 1 in Fig. 7 at 25 W with corresponding curves in Fig. 4 at 5 W and see the corresponding values of ΔT_{max} of 30 and 21 °C in Table 1. This small temperature difference in vertical direction is quite surprising considering the higher temperature level in the boiling case of Fig. 7. Even the thermocouples at the bottom and closest to the end of the pipe in Fig. 7 (3○ and 3△, see Fig. 7b) registered temperatures over 70 °C, at times exceeding 25 s. With 15 W, maximum temperatures at the same positions were below 58 °C and in with 5 W under 43 °C (not shown, see Appendix A), while the temperature differences in vertical direction were even less than the 5 degrees of Fig. 7 discussed above.

Visual observations clarify the above temperature fluctuations. Because of the high temperatures around the fiber tip, new boiling bubbles readily appear that are clearly visibly in water. Detachment frequency is observed to be about 0.8 Hz. This intensive boiling process intensifies the convective motion already induced by

Fig. 6. Left: photograph of vapor bubbles occurring in water with a bare tip at 2 mm/s and relatively high laser power (25 W). Right: schematic showing the biggest bubbles as well as the position of the fiber tip.

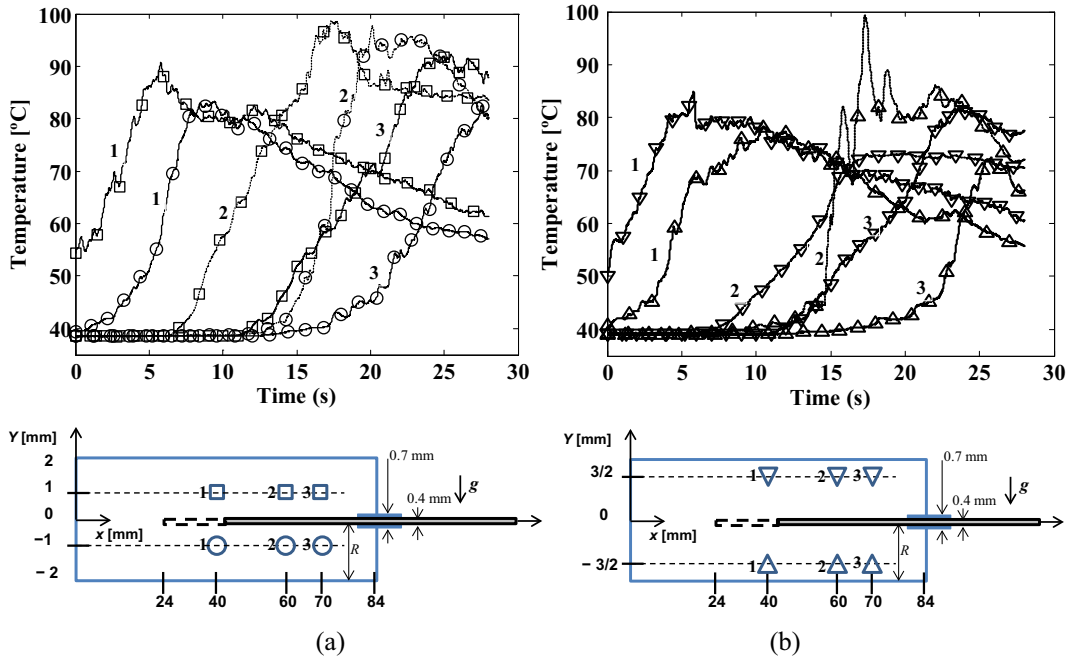

Fig. 7. Temperature histories measured in water with a bare fiber tip at high power (25 W) and with pullback speed of 2 mm/s. Figure (a) shows those relatively close to the centerline, at positions $y/R = +0.5$ and -0.5. Figure (b) those further away from the centerline, at positions $y/R = +0.75$ and -0.75.

the buoyancy effects owing to large temperature gradients in the water. As usual with detaching boiling bubbles, the temperature field is fairly homogeneous and close to the saturation temperature in the entire volume, as can be seen in Fig. 7. The increased mixing that accompanies boiling explains the relatively small temperature gradients found everywhere; these small gradients follow from the proximity of temperatures in Fig. 7 at locations 1□, 1○, 1▽ and 1△ after 10 s, for example. Similar observations hold for the couples at positions 2 and 3, but starting at later times of course.

3.2.2. Typical temperature histories in water with a fiber tip with carbonized layer, 15 or 25 W

The effect of a laser light irradiated carbonized layer on the tip of a fiber is clearly illustrated by the observations of Fig. 8. Submer-

Fig. 8. A fiber tip held in a pool of water at room temperature with 15 W laser irradiation. With a bare tip (a) boiling is not observed while with a carbonized layer (b) boiling is clearly visible.

sion during ten seconds yielded a visible boiling phenomenon at the carbonized tip (Fig. 8b). No boiling occurred at the bare tip (Fig. 8a). The carbonized layer absorbs 55% of the energy provided at the fiber tip ([15]). The extent of the channel volume directly heated by laser light emanating from the fiber tip is primarily determined by radiation absorption in the fluid; see Poluektova et al. [28]. Heat conduction from the fiber tip, if it is carbonized and hot, is a second important mechanism of heat transfer to the fluid. Heating of the fluid close to the tip by conduction adds to the heating by radiation and causes the temperature rise to be more localized near the fiber tip (Poluektova et al. [28]). As a result, the carbonized layer promotes boiling.

Typical temperature histories with a carbonized fiber tip in water at 15 W laser power and 2 mm/s pullback speed are presented in Fig. 9.

With 15 W and 25 W boiling occurred more intensely than in the corresponding water cases with a bare tip. With detaching boiling bubbles and intense mixing, the temperature field becomes quite homogeneous, as can be seen from the proximity of temperatures at 1□ and 1○ after 12 s in Fig. 9 and from Table 1, where the ΔT_{max} and *Gr* are smaller for carbonized tips than for bare tips.

3.2.3. Typical temperature histories in blood with an initially bare fiber tip at 4 mm/s, 5 and 10 W

Measurements with blood could be achieved at a pullback speed of 4 mm/s and a laser power of 5, 10 and 15 W; see the main results in Appendix A. Those with 5 and 10 W are discussed in the present section. Typical temperature histories at 5 W are presented in Fig. 10a and b. No carbonized layer was initially placed on the fiber tip but carbon layers are gradually being formed on the fiber tip once the laser is activated.

With 5 W, the temperature gradients in blood are similar to those in water with a bare fiber, *i.e.* without a carbonized layer, at the same pullback speed (Table 1: 20 and 16 °C). Consequently, the Grashof numbers are similar (7 and 6). Calculations have already shown [28] that two heat sources contribute about equally to the increase of the temperature on top of the tube, representative of the blood vessel wall in EVLA:

- the exceedingly hot fiber tip,
- the hot blood surrounding the fiber tip, heated up by direct absorption of the emitted laser light out of the tip.

Absorption in blood might be higher by a factor of about 10 than in water, see Section 2.2 (Fig. 2), but the strong conduction of heat from the very hot fiber tip in the case of a carbonized fiber tip, in water as well as in blood, compensates for the lower absorption of laser light in water. This driving force for convection is therefore about the same in blood as in water with a carbonized fiber tip.

Temperatures in the bottom half of the pipe level off in time and become more or less constant *in time*. The same leveling off is observed at 15 W, see also Fig. 11 discussed in Section 3.3. This result is explained from the relatively high heat release per unit of volume. Whereas at lower heat releases hot temperatures only occur when the hot probe passes by, the entire confined volume is more or less heated in stratified layers at these high heat release levels. The hot fluid stays on top and the fluid near the bottom stays hot because little heat can diffuse away from it.

3.3. Temperature and flow fields with gas bubbles at 4 mm/s, 15 W

At some times, the typical temperature profiles at 15 W shown in Fig. 11 exceed the saturation temperature of blood by far. This is probably the consequence of the occurrence of a big gas bubble that sticks to the fiber tip and is partly visible as an area that emits much more light than the area around it. Laser light is hardly absorbed in this gas bubble and irradiates directly on the thermocouple; the reading of the thermocouple might therefore be not a blood temperature. Additionally, these peak temperatures merely occur near the centerline. The temperatures further away from the centerline (Fig. 11b) are all quite similar; only those near the fiber tip are extremely high. These temperatures can become so high that an intense yellow light (Planck's radiation) was emitted from the fiber tip. The light emission moved along with the fiber tip. This light emission occurred only during some of the measurements at 15 W. This phenomenon is explained as follows.

A gas pocket at the fiber insulates the fiber tip and prevents cooling by the blood. The carbon layer that was deposited on the fiber tip heats up strongly through absorption of light even to temperatures high enough to cause melting of the silica. This melting has actually been observed at 25 W. Also in clinical situations melting of fibers has been reported [18].

Although gas bubbles occur in the boiling of blood, visual observations show that these bubbles strangely enough do not seem to detach in the measurements of Fig. 11. A possible explanation is given by Marangoni convection. High temperature gradients near the fiber tip make it possible for a gradient to occur in the surface tension coefficient at the interface of the bubble, provided the composition of the bubble is multicomponent. Marangoni flow around a bubble adhering to a hot plate is always directed away from the hot surface and presses the bubble towards the surface, see van der Geld et al. [29]. Other major forces tend to balance one another and will not lead to detachment unless a different force comes into play, see van der Geld et al. [30]. To substantiate the explanation with Marangoni convection, it needs to be proven that the content of the gas bubble is multicomponent.

The content of the gas bubbles has therefore been analyzed for its composition. The gas samples were extracted with a syringe and injected in a sample bag. A syringe filter (FH0206-1 Whatman 30 mm, 0.45 μm permeability) warranted that no blood entered the sample bag. Samples were then sealed off and cooled down.

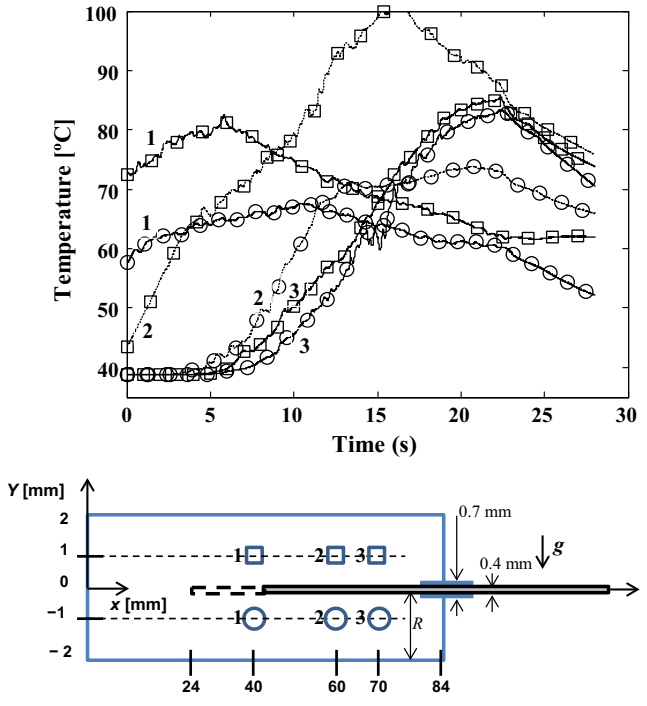

Fig. 9. Temperature histories measured in water with a fiber tip with a carbon layer at intermediate power, 15 W; pullback speed is 2 mm/s. Positions are relatively close to the centerline, at positions $y/R = +0.5$ and -0.5.

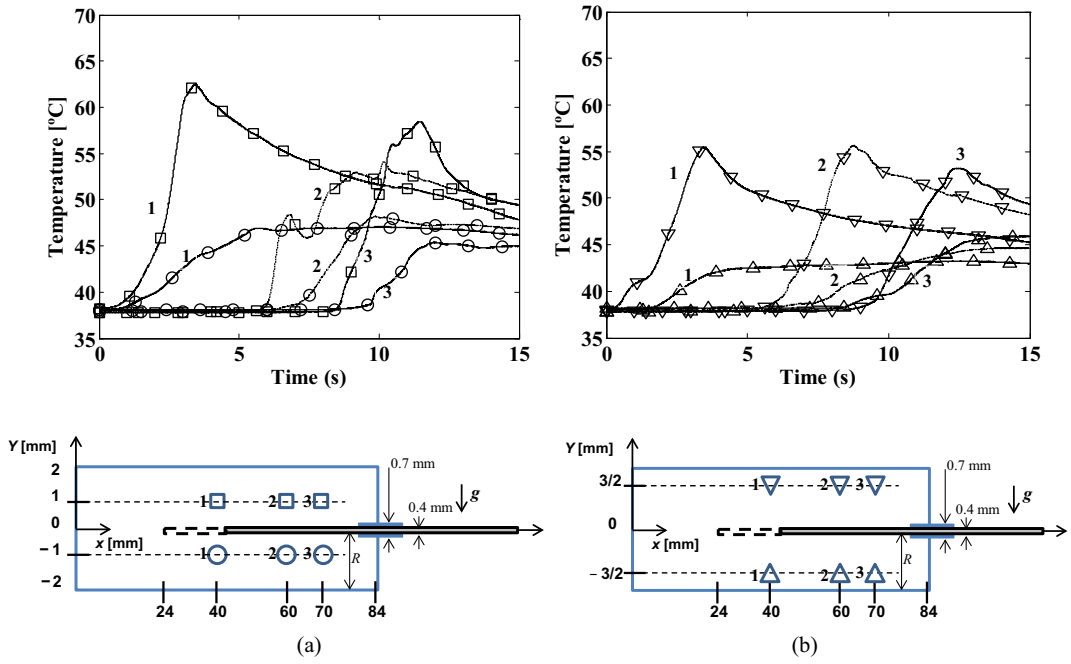

Fig. 10. Temperature histories measured in blood with an initially bare fiber tip at low power (5 W). Figure (a) shows those relatively close to the centerline, at positions $y/R = +0.5$ and -0.5. Figure (b) those further away from the centerline, at positions $y/R = +0.75$ and -0.75.

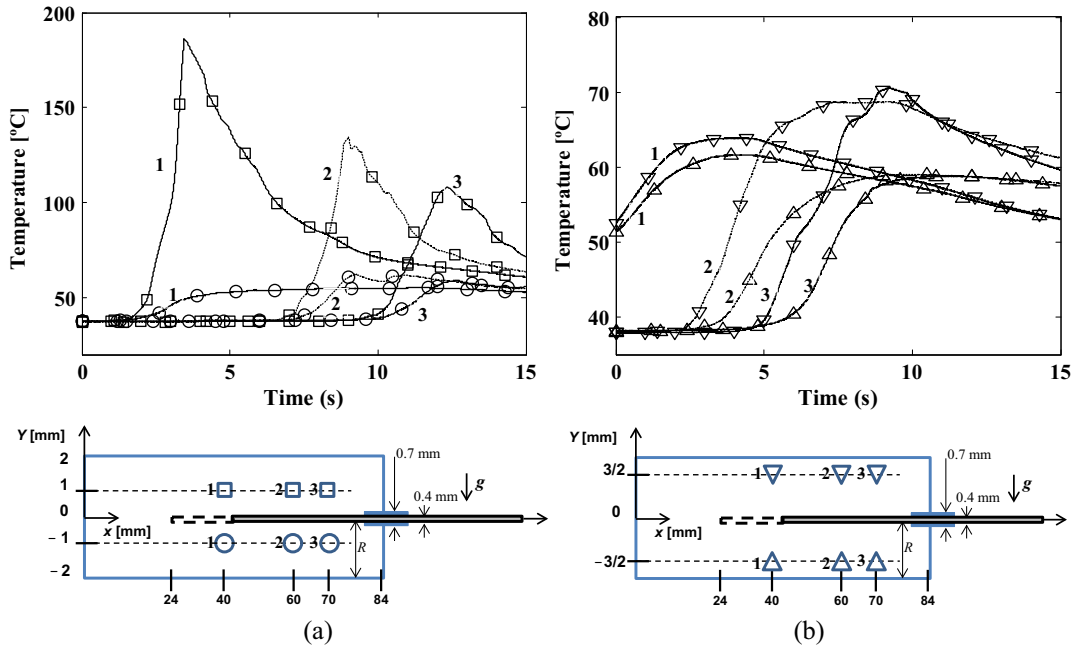

Fig. 11. Temperature histories measured in blood with an initially bare fiber tip at intermediate power (15 W). Figure (a) shows those relatively close to the centerline, at positions $y/R = +0.5$ and -0.5. Figure (b) those further away from the centerline, at positions $y/R = +0.75$ and -0.75.

Subsequent chemical analysis with a Shimadzu gas chromatograph with a mass spectrometer showed the occurrence of multiple fractions of carbon-oxides and hydrocarbons; see Table 2. The estimation of the molar fraction of CO is rough owing to the similar molecular weight of N_2. Air occurs because it dissolves into blood or as sample contamination or both. The remaining gases include other hydrocarbons, acetone and others.

Although the Grashof number for the blood case with 15 W is moderate (about 14, see Table 1), the temperature differences everywhere outside the gas bubble area are lower than those of the corresponding water cases at 15 W, see for example the equally numbered histories of Fig. 11b. Outside the core of the tube, temperatures are even more homogeneous in vertical direction than in the blood boiling case of Fig. 10.

4. Discussion

The fluid motion and temperatures created by the passage of a point light heat source moving along the central axis of a small

Table 2
Molar fractions of gas bubble components averaged over eight experiments with pig blood.

Components	Average molar fraction
CO_2	22.13
CO	19.05[a]
Vapor of H_2O	13.13[b]
C_3H_6	5.73
C_2H_4	4.80
Air[c]	3.82
C_2H_2	3.52
CH_4	3.05
C_3H_4	1.69
Remaining	23.08

[a] This amount is only a rough estimation, since N_2 content can also be included in the CO average molar fraction.
[b] This quantity may be higher in the gas bubble because of losses by condensation while processing the samples.
[c] All components with molecular weight of about 32.

tube in a confined volume have been studied in water and blood and with and without phase change occurring. An important application is EVLA treatment, as hazardous conditions must be avoided in this treatment; the present research contributes to the characterization and interpretation of these conditions.

Without boiling the convection patterns induced in water are close to those in blood. Buoyancy induces flow and axial mixing, as revealed by the high Grashof numbers that were experimentally assessed. Stratification occurs both in water and blood.

With boiling, notable temporal fluctuations in local temperatures occur. A carbonized layer on the fiber tip promoted boiling in water. Boiling bubbles in water rapidly detach from the tip and promote mixing and a homogeneous temperature field. When boiling blood, a gas bubble may be formed that sticks to the fiber tip (at 15 W and 4 mm/s); our explanation for this phenomenon is the occurrence of Marangoni convection. The fiber tip then

Table A1
Thermocouples on top of the fiber tip line but fairly close to it; 1, 2 and 3 label the downstream positions (pullback speed of 2 mm/s).

Experiment	$t_{rise,1}$	$t_{rise,2}$	$t_{rise,3}$	$t(T_{max,1})$	$t(T_{max,2})$	$t(T_{max,3})$	$T_{max,1}$	$T_{max,2}$	$T_{max,3}$
5 W; bare tip; water	−2	8	14	6	17	22	64	69	62
15 W; bare tip; water	−3	4	9	6	16	22	92	100	87
25 W; bare tip; water	−3	7	12	6	17	25	90	100	92
5 W; carbonized tip; water	0	9	15	6	17	23	68	77	69
15 W; carbonized tip; water	−6	−1	6	6	17	22	82	101	83
25 W; carbonized tip; water	−5	2	7	5	16	22	92	102	93

Table A2
Thermocouples below the fiber tip line, but fairly close to it; 1, 2 and 3 label the downstream positions (pullback speed of 2 mm/s).

Experiment	$t_{rise,1}$	$t_{rise,2}$	$t_{rise,3}$	$t(T_{max,1})$	$t(T_{max,2})$	$t(T_{max,3})$	$T_{max,1}$	$T_{max,2}$	$T_{max,3}$
5 W; bare tip; water	2	14	16	12	21	22	52	52	43
15 W; bare tip; water	2	10	16	7	20	23	72	70	58
25 W; bare tip; water	0	12	13	9	20	27	82	98	82
5 W; carbonized tip; water	2	12	17	20	27	27	47	48	44
15 W; carbonized tip; water	−5	4	6	11	21	23	67	73	82
25 W; carbonized tip; water	−5	6	7	11	21	26	74	90	96

Table A3
Thermocouples on top of the fiber tip line but more distant to it; 1, 2 and 3 label the downstream positions (pullback speed of 2 mm/s).

Experiment	$t_{rise,1}$	$t_{rise,2}$	$t_{rise,3}$	$t(T_{max,1})$	$t(T_{max,2})$	$t(T_{max,3})$	$T_{max,1}$	$T_{max,2}$	$T_{max,3}$
5 W; bare tip; water	−5	5	12	6	20	22	53	52	53
15 W; bare tip; water	−7	2	7	4	15	19	66	65	70
25 W; bare tip; water	−2	7	11	6	17	23	84	73	81
5 W; carbonized tip; water	−5	5	10	6	18	24	56	57	60
15 W; carbonized tip; water	−7	3	7	6	20	23	75	77	84
25 W; carbonized tip; water	−5	3	7	6	17	23	82	87	98

Table A4
Thermocouples below the fiber tip line but more distant to it; 1, 2 and 3 label the downstream positions (pullback speed of 2 mm/s).

Experiment	$t_{rise,1}$	$t_{rise,2}$	$t_{rise,3}$	$t(T_{max,1})$	$t(T_{max,2})$	$t(T_{max,3})$	$T_{max,1}$	$T_{max,2}$	$T_{max,3}$
5 W; bare tip; water	−2	8	14	12	21	27	47	48	43
15 W; bare tip; water	−1	7	11	7	18	19	57	63	47
25 W; bare tip; water	0	8	16	11	17	26	78	99	72
5 W; carbonized tip; water	0	10	15	20	27	27	44	47	44
15 W; carbonized tip; water	−3	8	12	12	21	25	54	66	75
25 W; carbonized tip; water	−2	9	11	7	17	25	64	73	80

Table A5
Thermocouples on top of the fiber tip line but fairly close to it; 1, 2 and 3 label the downstream positions (pullback speed of 4 mm/s).

Experiment	$t_{rise,1}$	$t_{rise,2}$	$t_{rise,3}$	$t(T_{max,1})$	$t(T_{max,2})$	$t(T_{max,3})$	$T_{max,1}$	$T_{max,2}$	$T_{max,3}$
5 W; bare tip; water	0	6	8	3	9	12	57	59	54
15 W; bare tip; water	0	5	8	3	9	12	74	88	76
25 W; bare tip; water	0	5	8	3	9	12	92	102	84
5 W; carbonized tip; water	−2	2	4	3	8	11	53	57	52
15 W; carbonized tip; water	−2	2	4	3	8	9	72	86	73
25 W; carbonized tip; water	−3	2	5	3	8	12	74	101	77
5 W; bare tip; blood	0	6	8	3	10	11	62	54	58
10 W; bare tip; blood	0	5	8	3	9	11	86	86	71
15 W; bare tip; blood	1	7	9	3	9	12	184	132	108

Table A6
Thermocouples below the fiber tip line, but fairly close to it; 1, 2 and 3 label the downstream positions (pullback speed of 4 mm/s).

Experiment	$t_{rise,1}$	$t_{rise,2}$	$t_{rise,3}$	$t(T_{max,1})$	$t(T_{max,2})$	$t(T_{max,3})$	$T_{max,1}$	$T_{max,2}$	$T_{max,3}$
5 W; bare tip; water	1	7	11	6	11	12	47	46	42
15 W; bare tip; water	1	7	11	6	11	12	62	63	56
25 W; bare tip; water	1	7	10	6	11	13	74	81	65
5 W; carbonized tip; water	−2	3	5	6	11	11	44	44	42
15 W; carbonized tip; water	−2	4	5	5	10	11	53	53	49
25 W; carbonized tip; water	−2	3	5	6	11	12	66	62	63
5 W; bare tip; blood	1	6	8	5	10	12	47	48	46
10 W; bare tip; blood	1	6	8	6	9	13	56	54	53
15 W; bare tip; blood	1	7	10	8	9	12	56	62	60

Table A7
Thermocouples on top of the fiber tip line but more distant to it; 1, 2 and 3 label the downstream positions (pullback speed of 4 mm/s).

Experiment	$t_{rise,1}$	$t_{rise,2}$	$t_{rise,3}$	$t(T_{max,1})$	$t(T_{max,2})$	$t(T_{max,3})$	$T_{max,1}$	$T_{max,2}$	$T_{max,3}$
5 W; bare tip; water	−1	3	5	3	9	10	47	46	47
15 W; bare tip; water	−2	3	5	3	9	10	56	54	57
25 W; bare tip; water	−1	3	5	3	9	10	70	67	73
5 W; carbonized tip; water	−1	4	7	3	9	11	49	49	51
15 W; carbonized tip; water	−2	2	5	3	8	9	57	64	75
25 W; carbonized tip; water	−2	3	5	3	9	11	85	73	81
5 W; bare tip; blood	0	5	8	3	9	13	55	56	53
10 W; bare tip; blood	−1	3	5	3	10	11	63	55	64
15 W; bare tip; blood	−2	2	4	3	8	9	64	68	70

Table A8
Thermocouples below the fiber tip line but more distant to it; 1, 2 and 3 label the downstream positions (pullback speed of 4 mm/s).

Experiment	$t_{rise,1}$	$t_{rise,2}$	$t_{rise,3}$	$t(T_{max,1})$	$t(T_{max,2})$	$t(T_{max,3})$	$T_{max,1}$	$T_{max,2}$	$T_{max,3}$
5 W; bare tip; water	−1	3	6	9	10	17	43	43	41
15 W; bare tip; water	−2	3	6	6	9	10	49	50	43
25 W; bare tip; water	−1	3	7	5	9	10	58	62	47
5 W; carbonized tip; water	0	5	8	11	16	16	42	42	41
15 W; carbonized tip; water	−2	4	6	7	11	11	48	51	57
25 W; carbonized tip; water	−2	4	7	5	8	12	78	92	68
5 W; bare tip; blood	1	5	8	12	14	16	43	45	46
10 W; bare tip; blood	−1	3	5	9	12	16	52	51	52
15 W; bare tip; blood	−2	2	4	4	10	11	62	58	57

may reach temperatures high enough to cause damage to the fiber [15], [18].

The main conclusions of this work are the following:

- Without boiling, convection patterns induced by a moving heat source in water are close to those in blood and buoyancy induced flow, axial mixing and temperature stratification occur.
- Boiling bubbles in water rapidly detach from the tip and promote mixing and a homogeneous temperature field.
- With boiling of blood, temperatures near the wall never reach 75 °C at a laser power of 15 W or less and a gas bubble may be formed that sticks to the fiber tip that might become damaged.

Acknowledgements

The authors gratefully acknowledge support of this work by the Brazilian National Council of Research (CNPq) through the project call "Science without borders", protocol number: Proc.

405700/2013-0. They also express their gratitude to Toine Stokbroekx for lending laser equipment, to Millán Lafuente for his help with the measurements and to Robin Doddema for performing the analysis of the gas content.

Appendix A. Tables of the main experimental results

The main experimental results are summarized in Tables A1–A8. The maximum temperatures at streamwise positions 1, 2 and 3 for various process conditions are represented by $T_{max,1}$, $T_{max,2}$ and $T_{max,3}$. The corresponding times of occurrence of this maximum temperatures are given by $t(T_{max,1})$, $t(T_{max,2})$ and $t(T_{max,3})$. The time lag between the start of the measurement and the first rise in temperature at positions 1, 2 and 3 are represented by $t_{rise,1}$, $t_{rise,2}$ and $t_{rise,3}$, respectively.

References

[1] D. Fultz, R.R. Long, G.V. Owens, W. Bohan, R. Kaylor, J. Weil, Met. Monograph 4 (21) (1959) 36.
[2] H. Rishbeth, Nature 229 (1971) 333.
[3] M.E. Stern, Tellus 23 (1971) 122.
[4] H.A. Douglas, P.J. Mason, E.J. Hinch, Motion due to a moving internal heat source, J. Fluid Mech. I54 (Part 3) (1972) 469–480.
[5] L.X. Yang, X.F. Peng, B.X. Wang, Numerical modeling and experimental investigation on the characteristics of molten pool during laser processing, Int. J. Heat Mass Transfer 44 (2001) 4465–4473.
[6] X.-H. Ye, X. Chen, Three-dimensional modeling of heat transfer and fluid flow in laser full-penetration welding, J. Phys. D: Appl. Phys. 35 (2002) 1049–1056.
[7] A. Karimipour, E. Abedini, H. Ajam, S.M.H. Sarvari, Modeling of fluid flow and heat transfer in laser welding with a moving heat source, Adv. Mater. Res. 622–623 (2013) 618–622.
[8] K. Mundra, T. DebRoy, K.M. Kelkar, Numerical prediction of fluid flow and heat transfer in welding with a moving heat source, Numer. Heat Transfer, Part A: Appl. 29 (2) (1996) 115–129.
[9] W.S.J. Malskat, A.A. Poluektova, C.W.M. van der Geld, H.A.M. Neumann, R.A. Weiss, C.M.A. Bruijninckx, M.J.C. van Gemert, Endovenous laser ablation (EVLA): a review of mechanisms, modeling outcomes, and issues for debate, Lasers Med. Sci. 29 (2014) 393–403.
[10] J. Pearce, S. Thomsen, Rate process analysis of thermal damage, in: A.J. Welch, M.J.C. van Gemert (Eds.), Optical-Thermal Response of Laser-Irradiated Tissue, Plenum Press, New York, 1995, p. 569.
[11] S.R. Mordon, B. Wassmer, J. Zemmouri, Mathematical modeling of 980-nm and 1320-nm endovenous laser treatment, Lasers Surg. Med. 39 (2007) 256–265.
[12] R.R. van den Bos, M.A. Kockaert, H.A.M. Neumann, R.H. Bremmer, T. Nijsten, M. J.C. van Gemert, Heat conduction from the exceedingly hot fiber tip contributes to the endovenous laser ablation of varicose veins, Lasers Med. Sci. 2009;24:247–251 (Erratum 2009; 24:679).
[13] R.M. Verdaasdonk, F.C. Holstege, E.D. Jansen, C. Borst, Temperature along the surface of modified fiber tips for Nd:YAGlaser angioplasty, Lasers Surg. Med. 11 (1991) 213–222.
[14] R.A. Weiss, Comparison of endovenous radiofrequency versus 810 nm diode laser occlusion of large veins in an animal model, Dermatol. Surg. 28 (2002) 56–61.
[15] M. Amzayyb, R.R. van den Bos, V.M. Kodach, D.M. de Bruin, T. Nijsten, H.A.M. Neumann, M.J.C. van Gemert, Carbonised blood deposited on fibers during 810, 940 and 1470 nm endovenous laser ablation: thickness and absorption by optical coherence tomography, Lasers Med. Sci. 25 (2010) 439–447.
[16] M. Vuylsteke, J. Van Dorpe, J. Roelens, T. De Bo, S. Mordon, I. Fourneau, Intraluminal fiber-tip centering can improve endovenous laser ablation: a histological study, Eur. J. Vasc. Endovasc. Surg. 40 (2010) 110–116.
[17] C.-M. Fan, R.R. Anderson, Endovenous laser ablation: mechanism of action, Phlebology 23 (2008) 206–213.
[18] B.C.V.M. Disselhoff, A.I. Rem, R.M. Verdaasdonk, D.J. der Kinderen, F.L. Moll, Endovenous laser ablation: an experimental study on the mechanism of action, Phlebology 23 (2008) 69–76.
[19] T.M. Proebstle, H.A. Lehr, A. Kargl, C. Espinola-Klein, W. Rother, S. Bethge, J. Knop, Endovenous treatment of the greater saphenous vein with a 940-nm diode laser: thrombotic occlusion after endoluminal thermal damage by laser-generated steam bubbles, J. Vasc. Surg. 35 (2002) 729–736.
[20] C.W.M. van der Geld, R.R. van den Bos, P.W.M. van Ruijven, T. Nijsten, H.A.M. Neumann, M.J.C. van Gemert, The heat-pipe resembling action of boiling bubbles in endovenous laser ablation, Lasers Med. Sci. 25 (2010) 907–909.
[21] C.M. Rops, G.J. Oosterbaan, C.W.M. van der Geld, Once-through contactless flow boiling in a micro evaporator, Interf. Phenom. Heat Transfer J. 2 (3) (2014) 265–271.
[22] C.M. Rops, G.J. Oosterbaan, C.W.M. van der Geld, A way to reduce the pressure drop in once-through micro evaporators, Exper. Heat Transfer 27 (4) (2014) 329–339.
[23] J.C. Passos, F.R. Hirata, L.F.B. Possamai, M. Balsamo, M. Misale, Confined boiling of FC72 and FC87 on a downward facing heating copper disk, Int. J. Heat Fluid Flow 25 (2004) 313–319.
[24] J.C. Passos, E.L. da Silva, L.F.B. Possamai, Visualization of FC72 confined nucleate boiling, Exp. Thermal Fluid Sci. 30 (2005) 1–7.
[25] Y.A. Cengel, Heat Transfer: A practical approach, second ed., McGraw-Hill, 2002, page 487.
[26] N. Bosschaard, G.J. Edelman, M.C.G. Aalders, T.G. van Leeuwen, D.J. Faber, A literature review and novel theoretical approach on the optical properties of whole blood, Lasers Med. Sci. 29 (2014) 453–479.
[27] G.M. Hale, M.R. Querry, Optical constants of water in the 200-nm to 200-μm wavelength region, Appl. Opt. 12 (1973) 555–563.
[28] A.A. Poluektova, W.S.J. Malskat, M.J.C. van Gemert, C.M.A. Bruijninckx, H.A.M. Neumann and C.W.M. van der Geld. Some controversies in Endovenous Laser Ablation of varicose veins addressed by optical-thermal mathematical modeling, Lasers Med. Sci., 2014, pp. 441–452.
[29] C.W.M. van der Geld, C. Colin, Q.I.E. Segers, V.H. Pereira da Rosa, H.N. Yoshikawa, Forces on a boiling bubble in a developing boundary layer, in microgravity with g-jitter and in terrestrial conditions, Phys. Fluids, 2012, 24 (8), 082104–1/29.
[30] C.W.M. van der Geld, C.H.M. Baltis, G.J.M. Priems, Forces in rapid vapor bubble growth in forced convection with varying angle of inclination, Colloids and Surfaces A: Physicochemical and Engineering Aspects, 2016, pp. 29–36.